Available online at www.sciencedirect.com

SciVerse ScienceDirect

Advances in Space Research 51 (2013) 1478–1491

Advances in Space Research
(a COSPAR publication)

www.elsevier.com/locate/asr

Transponder calibration of the Envisat RA-2 altimeter Ku band sigma naught

N. Pierdicca [a,*], C. Bignami [b,2], M. Roca [c,3], P. Féménias [d,4], M. Fascetti [a,1], M. Mazzetta [a,1], C.N. Loddo [e,5], A. Martini [e,5], S. Pinori [e,5]

[a] *Dept. of Information Engineering, Electronics and Telecommunications, Sapienza University of Rome, Via Eudossiana 18, 00186 Rome, Italy*
[b] *Istituto Nazionale di Geofisica e Vulcanologia, Via di Vigna Murata 605, 00143 Rome, Italy*
[c] *isardSAT, Parc Tecnològic BCNord, C. Marie Curie 8-14, 08042 Barcelona, Spain*
[d] *European Space Agency/ESRIN, Via Galileo Galilei, 00044 Frascati, Italy*
[e] *Serco S.p.a., Via Sciadonna, 24, 00044 Frascati, Rome, Italy*

Available online 22 December 2012

Abstract

Although the history of spaceborne altimeters goes back to the early seventies, the absolute calibration of the backscattering coefficient has never been deeply investigated. This information has been primarily used to infer the wind speed via an empirical model, and the intercalibration among different satellite altimeters has revealed to be suitable for this purpose, being the wind retrieval based on an empirical relationship. As far as Ku band system is concerned, the sigma naught absolute calibration of the Envisat altimeter (RA-2) has been performed using an active reference target provided by a transponder. This has been exploited during the 6-month Commissioning phase to generate early calibration results. In order to monitor the RA-2 backscatter calibration during the Envisat lifetime, a continuous calibration effort has been carried out by operating the transponder as much as possible. This paper aims to review the entire effort for calibrating the RA-2 sigma naught measurements, which lasted for almost seven years. It presents in detail the adopted methodology and the final outcome of the activity, providing the users with the correction (bias) to get the calibrated sigma naught and analyzing its stability during almost the entire Envisat lifetime. Specifically, it is concluded that the RA-2 backscatter measurements were quite stable, even if a bias of about 1 dB should be considered with respect to the actually released product. Some small changes in the bias as function of time can be identified during most of the Envisat lifetime, consisting in a slight increase in the first two years, followed by a more stable period and a final drop observed at the end of 2009, until the conclusion of the calibration activity (corresponding to the change in Envisat orbit).

Keywords: Radar altimeter; Envisat; External calibration; Backscattering coefficient; Transponder

1. Introduction

The Envisat satellite mission was developed by the European Space Agency (ESA) as successor to the European Remote Sensing (ERS) missions (ERS-1 and ERS-2) and launched in 2002. It carries ten sophisticated optical and radar instruments to provide continuous observation and monitoring of the Earth's land, atmosphere, oceans and ice caps. Unfortunately, the Envisat mission ended on 08 April 2012, following the unexpected loss of contact with the satellite. Even after the end of the mission, ten years of archived data from Envisat continue to be exploited for many studies. The achievements of the Envisat mission during its operation cover so many applications that it is difficult to provide a comprehensive list of

* Corresponding author. Tel.: +39 06 44585411; fax: +39 06 4742647.
E-mail address: nazzareno.pierdicca@uniroma1.it (N. Pierdicca).

[2] Tel.: +39 06 518601; fax: +39 06 5041181.
[3] Tel./fax: +34 93 350 55 08.
[4] Tel.: +39 06 94180951; fax: +39 06 94180280.
[5] Tel.: +39 06 98354400; fax: +39 06 941 9426.

0273-1177/$36.00 © 2012 COSPAR. Published by Elsevier Ltd. All rights reserved.
http://dx.doi.org/10.1016/j.asr.2012.12.014

references, so that the reader can refer to the ESA website (www.esa.int/envisat), or to the Proceeding of the IEEE International Geoscience and Remote Sensing Symposium (IGARSS) held in Munich on 2012 for the last updates.

The Radar Altimeter 2 (RA-2) on board of Envisat operates in two bands (Ku at 13.575 GHz, and S at 3.20 GHz), and is primarily conceived to measure the range to the Earth surface (Envisat Project team, 2001; Resti et al., 1999). By combining this information with accurate orbit data, it is possible to determine the surface level in a geocentric coordinate system (or with respect to a reference ellipsoid). In addition to this primary objective, RA-2 is capable of measuring other parameters of the surface, and in particular the backscattering coefficient (sigma naught, $\sigma°$) at nadir (zero degrees of incidence angle). Although the history of spaceborne altimeters goes back to the early seventies (Barrick and Swift, 1980), the calibration of the backscattering coefficient has never been deeply investigated. This information has been primarily used to infer the wind speed via an empirical model, and the intercalibration among different satellite altimeters has revealed to be suitable for this purposes, being the wind retrieval based on an empirical relationship (Faugere et al., 2006). However, further pieces of information can be gathered over ocean using backscatter measurements, such as gas transfer velocity derived by exploiting multifrequency observations (Frew et al., 2007), and altimetric surface wave period (Gommenginger et al., 2003). The quantitative information about short-scale wind wave roughness, wind stress and even atmospheric rainfall can exploit the differential behavior of the backscatter using multifrequency altimetric data (Quartly, 2000; Elfouhaily et al., 1998). Although relative calibration could be sufficient for exploiting differential algorithms, in practices most of these applications require well calibrated backscatter measurements.

Additionally, the question of the physical modeling of the sea scattering is still a scientific priority, especially for special radar configurations, such as specular (Yurchak, 2012) and bistatic geometry (Brogioni et al., 2010). Several investigations have been carried out to tackle the problem (Vandemark et al., 2004), to understand the coupled effect of wind and large scale roughness (Tran et al., 2007), and thus to improve the wind speed retrieval and the Sea Surface Bias (SSB) as well (Gourrion et al., 2002). For these purposes, direct calibrated observations from satellite can be very useful, if accuracy can reach 0.4 dB and possibly 0.2 dB. They would be also important to exploit a combination of altimetric backscatter measurements with slanted observations from scatterometers, and emissivity from microwave radiometers. In addition, an interest in monitoring the nadir backscattering over land is emerging. It may contribute to a better intercalibration of multimission altimeter sigma naught measurements, especially over desert and very dry and stable areas, as done in (Bramer et al., 2005), who produced a reference sigma naught map of the test area interpolating re-tracked backscatter values from ERS-1/2 missions, and then compared it with backscatter tracks from other altimetric missions. Nadir backscatter from altimeter over land have been also studied for the purpose to monitor different surface characteristics at regional and global scale, exploiting the sensing capabilities of the nadir looking geometry with respect to side looking radars, and the availability of a long time series of altimetric missions which balances the poor spatial sampling of the altimeter. In particular in (Yang et al., 2010) a large altimeter data set as been jointly processed to produce a land cover map of China. Bramer and Berry (2010) have used altimeter backscatter to monitor soil moisture, whereas in (Ridley et al., 1996) the nadir backscatter from a desert area has been analyzed both theoretically and experimentally. Papa et al. (2002) and Papa et al. (2003) demonstrated the potential of altimeter backscatter measurements in different fields of land monitoring, such as snow pack, vegetation parameter retrievals, and especially to estimate the extent and seasonality of northern wetlands (Papa et al., 2006).

Up to now, the calibration of the different satellite missions has been proven to differ for amounts that can reach 2.75 dB (Karaev et al., 2006; Queffeulou, 2003). A careful intercalibration of Jason-1 and RA-2 Envisat has been carried out in (Tran et al., 2005), exploiting also the data from the TRMM Precipitation Radar Measurements. Quartly (2000) has developed a method to monitor the altimeter's backscatter by assessing the correlations between the values at two different frequencies. None of the above works has faced the problem of absolute and independent external calibration.

From engineering point of view, the calibration of sigma naught requires the exact knowledge of all the instrument and observation parameters that appear in the radar equation. They include transmitted power, antenna gain pattern, range and pointing angle, receiver characteristics. During the on-ground testing, the RA-2 has been rather well characterized to ensure its performance in orbit, and this information is used in ground processing to invert the radar equation and to calculate sigma naught. As the accuracy of some of these parameters may not be enough for the purpose of sigma naught calibration and/or they may change during the flight, a proper calibration strategy has to be implemented.

In addition to an internal calibration loop, which does not include some subsystems (like the antenna), an external calibration can be performed by observing radar targets of a well-known radar cross section σ or an extended surface of known sigma naught $\sigma°$. Moreover, the *Passive Calibration* technique is based on the main assumption that the antenna and the transmitter characterization errors are of minor importance with respect to receiver errors. If the altimeter operates in "noise-listen" mode, i.e., detecting only the radiation emitted by the observed scenario in the absence of radar echo, the receiver response function can be characterized by techniques similar to those used for spaceborne radiometers (Pierdicca et al., 2006).

As far as Ku band is concerned, the $\sigma°$ absolute calibration of the RA-2 has been performed using a reference target provided by a transponder (TPD) that has been developed at the European Space Research and Technology centre (ESTEC) of ESA, in Noordwijk. This has been exploited during the 6-month Commissioning phase to generate early calibration results (Jackson 2002; Roca et al., 2003). In order to consolidate these calibration results and to monitor the RA-2 calibration of $\sigma°$ during the Envisat lifetime, a continuous monitoring activity was performed by operating the transponder as much as possible (Fèmènias et al., 2004; Martini et al., 2006).

This paper aims to review the entire effort for calibrating the RA-2 sigma naught measurements, which lasted for almost seven years. It presents in detail the proposed methodology and the final outcome of the activity, providing the users with the correction (bias) to get the calibrated sigma naught and analyzing its stability during almost the entire Envisat lifetime. Note that, although we have adopted a mathematical formalism which refers to the Envisat RA-2 instrument and processing specification documents, the transponder calibration approach described here can be applied to other missions, like the Ocean Surface Topography Mission (OSTM) (Bannoura et al., 2005), and especially it could be envisaged for the upcoming Sentinel 3 mission developed by ESA (Seitz et al., 2010).

In Section 2 we provide an overview of the performed activity, introduce the equations governing the power at the altimeter output and describe the algorithms to estimate the correction (given as a bias) to the nominal sigma naught product. Section 3 gives an overview of the estimated bias during the Envisat mission lifetime and discusses the main outcomes of such a long term monitoring. Section 4 draws the main conclusions, including the recommendations emerging from this experience for future calibration of upcoming altimetry missions.

2. RA-2 sigma naught calibration activity summary

The transponder has been developed at ESA ESTEC, and fully characterized and calibrated on an open range, using a reference target plate placed at about 250 m from the TPD, leading to a final estimate of the Radar Cross Section (RCS) of 75.08 dBm^2 and to elevation and azimuth cuts of the antenna beam. More details about the device characteristics and calibration are provided in (Jackson, 2002). Performing the external calibration by a TPD requires operating RA-2 in the so-called Preset Loop Output (PLO) when it overflies the calibration site. It means that the receiving time window has to be shifted in time with respect to the expected return from the Earth surface. The shift depends on the height of the calibration site and the time delay implemented into the TPD between the RA-2 signal arrival and the emission of the pulse replica. Such a delay was set to 55.088 μs in our case (Jackson, 2002). In this way the TPD signal received by RA-2 is isolated from the Earth echo.

During a preliminary phase of Envisat operations (about 18 months) the transponder has been deployed in different sites along the satellite tracks (*non-permanent* sites). Four orbits have been selected, whose ground tracks were not far from ESA-ESRIN establishment (Frascati, Italy). The TPD, which was mounted on a trail, has been regularly towed to the sites before each satellite pass. A careful positioning was carried out each time to ensure a correct pointing of the TPD antenna, not only in elevation (perfect zenith pointing), but also in azimuth, in order to ensure a suitable polarization matching with the RA-2 antenna. The elevation angle was adjusted mechanically by acting on the TPD supporting basement. It was used a precision leveling tool on top of the horn antenna aperture plane, placed alternatively along two orthogonal directions until an accurate horizontal leveling was reached. The azimuth adjustment was performed by identifying from the beginning in each site a reference point (RP), far enough but still well visible from the TPD, whose azimuth alignment with the TPD was measured by a differential GPS campaign. The TPD platform, which has azimuth rotation capability, was rotated in order to reproduce the same alignment with the RP at each calibration campaign, with the help of its sight device. Then it was rotated again in azimuth of the angle required to align the polarization of the two antennas. All these operations were performed using the motorized azimuthally rotating platform of the TPD electronic units. Following to the *non-permanent* site phase, a *permanent* site has been considered for operating the transponder for the rest of the Envisat lifetime. This has ensured acquisition of calibration data only each 35 days (the Envisat orbital cycle).

The activity foresaw not only the deployment and operation of the TPD, but also the selection of the most suitable sites along the satellite orbit and their preparation in order to host the TPD, both routinely (non-permanent sites) and permanently. The calibration effort has involved many actors, including the team working in the field to operate the transponder, ESA staff to program the satellite, researchers involved in the data processing and in the analysis of the results. In Fig. 1 the upper panel displays the locations of the transponder during the non-permanent phase, from February 24th, 2004 to October 4th, 2005. The four sites have been selected along the satellite tracks 208, 315, 437, and 43 according to logistic considerations, including ease and reliable access permissions and lack of nearby potential reflectors able to generate a return delayed with respect to that of the nadir point, thus superimposing to the delayed TPD pulse. The sites were located inside or near the towns of Maccarese, Rome, Valmontone and Fiuggi, respectively, as shown in Fig. 1. The permanent site was chosen once it was confirmed the availability of the Scuba Diver Team, of the Italian Fire Brigade, to host the TPD on top the terrace of its premises in Rome, which is located just along Envisat track 315, as shown in the lower panel of Fig. 1. Since October 2005 the TPD has been regularly operated at each Envisat overpass, until

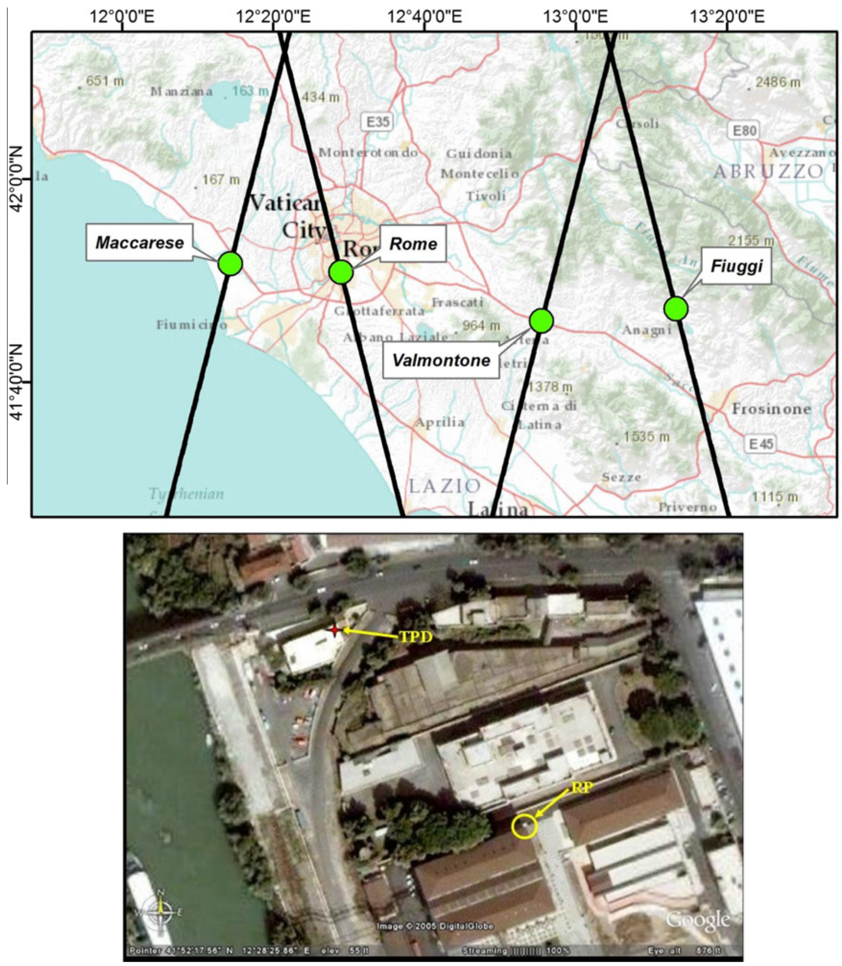

Fig. 1. Upper panel: non-permanent site locations, where the TPD has been moved each ENVISAT overpass (orbits 43, 208, 315, 437), from February 24th, 2004 to October 4th, 2005. Lower panel: location of the TPD during the permanent site phase, when the TPD was hosted by the Scuba Diver Team, Italian Fire Brigade in Rome, since October 2005 (ENVISAT orbit 315). The picture shows the TPD position and the Reference Point (RP) considered to align in azimuth the transponder antenna in order to match the RA-2 polarization.

the change of the Envisat orbit, which occurred on October 2010, and hampered the continuation of the activity.

Since the activity kick off (February 2004) up to the end of the mission, a total of 105 RA-2 acquisitions in PLO mode over the TPD sites have been planned. More than the 64% of the planned acquisitions have been successfully carried out and the bias evaluation was successfully computed. Unfortunately, the remaining 36% did not furnish useful data for the calibration due to different kinds of problems. They mainly originated from adverse meteorological conditions and occasional TPD failure and/or TPD anomalous behavior (especially failure of the loop which automatically control the TPD internal attenuation). In a few cases failures were due to Envisat planning or macrocommand problems (including errors in RA-2 Preset Loop timing), or other problems at the site (e.g., unattainability of the permanent site because of fireman emergency calls), or at the data processing facility. A total of 67 apparently reliable bias estimations have been successfully derived: 14 in RA-2 LOW resolution mode and 53 in HIGH resolution mode (those modes correspond to a different bandwidth of the altimeter transmitted chirp, which is 80 MHz and 320 MHz, respectively). Table 1 summarizes the overall activity, including absolute orbit number, time of each planned calibration, site and track number, RA-2 resolution mode, estimated atmospheric losses, and value of the estimated bias, as well as reason for failure of the calibration, whatever applicable.

3. The RA-2 external calibration approach

3.1. The radar altimeter in normal operation (tracking mode)

Fig. 2 shows the schematic diagram we have considered for RA-2 during normal operation, which was taken from RA-2 developer technical specifications, but can be extended to other altimeter sensors as well. Symbols A and AGC represent attenuation values, whilst symbol G is used to represent gain values. AGC_{sig} is the attenuation of the step attenuator inside the receiver, which is continuously set through an Automatic Gain Control (AGC) loop.

Table 1
Operational activity summary.

Absolute orbit	Date of measurement	Location/Rel. track	RA-2 resolution	Tropo Att. (one way) dB	Bias (dB)
10389	24-Feb-04	Rome 315	Low	0.06	1.082
10511	04-Mar-04	Valmontone/437	Low	0.051	1.054
10618	11-Mar-04	Fiuggi/43	Low	0.068	1.002
10783	23-Mar-04	Maccarese/208	Low	0.071	1.061
10890	30-Mar-04	Rome/315	Low	0.076	1.014
11012	08-Apr-04	Valmontone/437	High		No acquisition
11119	15-Apr-04	Fiuggi/43	High	0.061	1.085
11284	27-Apr-04	Maccarese/208	High		No acquisition
11391	04-May-04	Rome/315	High		No acquisition
11513	13-May-04	Valmontone/437	Low	0.067	0.926
11620	20-May-04	Fiuggi/43	Low	0.069	1.006
11785	01-Jun-04	Maccarese/208	High		No acquisition
11892	08-Jun-04	Rome/315	Low	0.077	1.108
12014	17-Jun-04	Valmontone/437	Low	0.174	1.256
12121	24-Jun-04	Fiuggi/43	Low	0.075	1.185
12286	06-Jul-04	Maccarese/208	Low		TPD failure
14290	23-Nov-04	Maccarese/208	Low	0.082	1.144
14397	30-Nov-04	Rome/315	Low	0.071	0.812
14519	09-Dec-04	Valmontone/437	Low	0.124	1.068
14626	16-Dec-04	Fiuggi/43	High		rainy
14791	28-Dec-04	Maccarese/208	High	0.067	1.104
14898	04-Jan-05	Rome/315	High	0.057	1.064
15020	13-Jan-05	Valmontone/437	High	0.059	0.998
15127	20-Jan-05	Fiuggi/43	High	0.054	1.118
15292	01-Feb-05	Maccarese/208	High	0.066	1.082
15399	08-Feb-05	Rome/315	High	0.062	1.174
15521	17-Feb-05	Valmontone/437	High	0.058	1.055
15628	24-Feb-05	Fiuggi/43	High		Snowy
15793	08-Mar-05	Maccarese/208	High	0.058	1.046
15900	15-Mar-05	Rome/315	High	0.064	1.058
16022	24-Mar-05	Valmontone/437	High	0.077	1.094
16129	31-Mar-05	Fiuggi/43	High		No acquisition
16294	12-Apr-05	Maccarese/208	High	0.07	1.110
16401	19-Apr-05	Rome/315	High	0.067	1.124
16523	28-Apr-05	Valmontone/437	High	0.057	1.084
16630	05-May-05	Fiuggi/43	High		No acquisition
16795	17-May-05	Maccarese/208	High	0.084	1.008
16902	24-May-05	Rome/315	High	0.076	1.152
17131	09-Jun-05	Fiuggi/43	High		No acquisition
17296	21-Jun-05	Maccarese/208	High		Attenuation Set. Error
17403	28-Jun-05	Rome/315	High	0.08	1.290
17525	07-Jul-05	Valmontone/437	High	0.065	1.170
17632	14-Jul-05	Fiuggi/43	High		No acquisition
17797	26-Jul-05	Maccarese/208	High		RA-2 command error
17904	02-Aug-05	Rome/315	High	0.094	1.208
18026	11-Aug-05	Valmontone/437	High	0.077	1.084
18133	18-Aug-05	Fiuggi/43	High		No acquisition
18298	30-Aug-05	Maccarese/208	High		Attenuation Set. Error
18405	06-Sep-05	Rome/315	High	0.08	1.220
18527	15-Sep-05	Valmontone/437	High	0.065	Problems at Kiruna station
18634	22-Sep-05	Fiuggi/43	High	0.076	1.152
18799	04-Opt-05	Maccarese/208	High	0.082	1.014
18906	11-Opt-05	ROMA-VVFF/315	Low	0.078	1.216
19407	15-Nov-05	ROMA-VVFF/315	High	0.095	1.279
19908	20-Dec-05	ROMA-VVFF/315	High		Mission planning problem
20409	24-Jan-06	ROMA-VVFF/315	High	0.055	1.470
20910	28-Feb-06	ROMA-VVFF/315	High	0.062	1.104
21411	04-Apr-06	ROMA-VVFF/315	High		Firemen emergency call
21912	09-May-06	ROMA-VVFF/315	High	0.069	1.138
22413	13-Jun-06	ROMA-VVFF/315	High		RA-2 SIDE B
22914	18-Jul-06	ROMA-VVFF/315	High		Attenuation Set. Error
23415	22-Aug-06	ROMA-VVFF/315	High		Attenuation Set. Error

(*continued on next page*)

Table 1 (*continued*)

Absolute orbit	Date of measurement	Location/Rel. track	RA-2 resolution	Tropo Att. (one way) dB	Bias (dB)
23916	26-Sep-06	ROMA-VVFF/315	High	0.086	1.232
24417	31-Opt-06	ROMA-VVFF/315	High	0.071	1.223
24918	05-Dec-06	ROMA-VVFF/315	High	0.078	1.156
25419	09-Jan-07	ROMA-VVFF/315	High	0.074	1.117
25920	13-Feb-07	ROMA-VVFF/315	High	0.059	1.190
26421	20-Mar-07	ROMA-VVFF/315	High		Rainy
26922	24-Apr-07	ROMA-VVFF/315	High	0.077	1.324
27423	29-May-07	ROMA-VVFF/315	High	0.084	1.208
27924	03-Jul-07	ROMA-VVFF/315	High		Attenuation Set. Error
28425	07-Aug-07	ROMA-VVFF/315	High		Attenuation Set. Error
28926	11-Sep-07	ROMA-VVFF/315	High		Firemen emergency call
29427	16-Opt-07	ROMA-VVFF/315	High		Attenuation Set. Error
29928	20-Nov-07	ROMA-VVFF/315	High	0.0697	1.179
30429	25-Dec-07	ROMA-VVFF/315	High		No campaign
30930	29-Jan-08	ROMA-VVFF/315	High	0.0668	1.144
31431	04-Mar-08	ROMA-VVFF/315	High	0.0695	1.179
31932	08-Apr-08	ROMA-VVFF/315	High		No operation:rain
32433	13-May-08	ROMA-VVFF/315	High	0.0879	0.87
32934	17-Jun-08	ROMA-VVFF/315	High		No operation:rain
33435	22-Jul-08	ROMA-VVFF/315	High	0.0678	1.136
33936	26-Aug-08	ROMA-VVFF/315	High		Attenuation Set. Error
34437	30-Sep-08	ROMA-VVFF/315	High		Attenuation Set. Error
34938	04-Nov-08	ROMA-VVFF/315	High		No operation:rain
35439	09-Dec-08	ROMA-VVFF/315	High	0.0729	0.98
35940	13-Jan-09	ROMA-VVFF/315	High		No operation:rain
36441	17-Feb-09	ROMA-VVFF/315	High	0.0803	0.97
36942	24-Mar-09	ROMA-VVFF/315	High	0.084	0.89
37443	28-Apr-09	ROMA-VVFF/315	High		RA-2 anomaly
37944	02-Jun-09	ROMA-VVFF/315	High	0.0683	1.012
38445	07-Jul-09	ROMA-VVFF/315	High	0.19	TPD test set
38946	11-Aug-09	ROMA-VVFF/315	High		Attenuation Set. Error
39447	15-Sep-09	ROMA-VVFF/315	High		Bias processing problem
39948	20-Opt-09	ROMA-VVFF/315	High	0.071	1.06
40449	24-Nov-09	ROMA-VVFF/315	High	0.0707	0.9
40950	29-dec-09	ROMA-VVFF/315	High	0.1213	0.76
41451	02-Feb-10	ROMA-VVFF/315	High	0.0773	0.83
41952	09-Mar-10	ROMA-VVFF/315	High		No operation:rain
42453	13-Apr-10	ROMA-VVFF/315	High	0.0713	0.893
42954	18-May-10	ROMA-VVFF/315	High	0.0797	0.889
43455	22-Jun-10	ROMA-VVFF/315	High	0.0907	0.921
43956	27-Jul-10	ROMA-VVFF/315	High	0.0837	0.917
44457	31-Aug-10	ROMA-VVFF/315	High	0.0632	0.946
44958	05-Opt-10	ROMA-VVFF/315	High	0.085	1.220

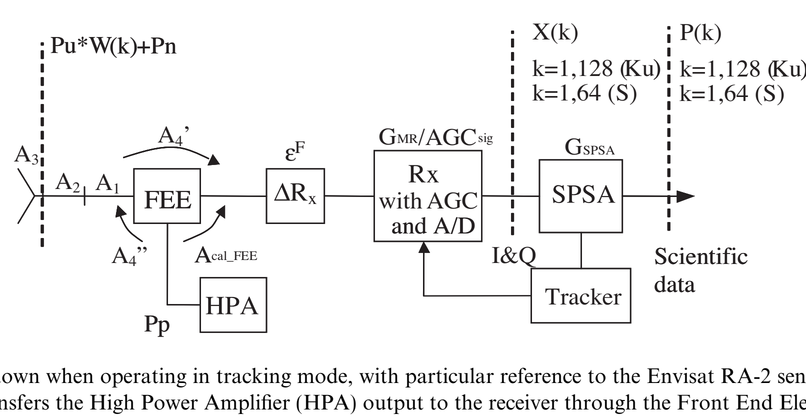

Fig. 2. Radar altimeter breakdown when operating in tracking mode, with particular reference to the Envisat RA-2 sensor. Note that an internal loop is foreseen which periodically transfers the High Power Amplifier (HPA) output to the receiver through the Front End Electronics (FEE) to perform the so called Point Target Response (PTR) calibration.

A_4', A_4'', and A_{cal_FEE} are the attenuations of the Front End Electronic (FEE) between the different paths of the three-port device. A_1 and A_2 are attenuations of the wave-guides and A_3 is the attenuation introduced by the antenna (to which we can refer also as the inverse of the antenna efficiency). P_p is the output power of the High Power Amplifier (HPA). The gain of the receiver R_x is indicated with G_{MR}/AGC_{sig}, (G_{MR} is the microwave receiver gain) to put in evidence the variable attenuation AGC_{sig}. At the output of the analog receiver, after A/D conversion, we have the I&Q complex samples. The scientific data $P(k)$, that are the altimeter output waveforms, are composed of 128 samples ($k = 1,...128$) for Ku band and 64 samples ($k = 1,....64$) for S band in the specific case of RA-2. They are produced by the digital Signal Processing Sub Assembly (SPSA). This module, with gain G_{SPSA}, performs the FFT, square detection and accumulation over 100 return echoes for Ku channel (25 for S channel). The block ΔR_x has been also introduced to account for in-flight changes of the analog receiver with respect to the nominal receiver R_x, as it has been characterized on ground. ε^F is the gain of module ΔR_x, i.e., the variable and unknown factor of the receiver gain that is monitored on board by the internal calibration loop, to which it is referred as Pulse Transfer Response (PTR) calibration.

At the output of the instrument, the samples of the detected signal $P(k)$ are given by the power received by the antenna multiplied by the gain of the overall receiver chain. The superimposed noise power P_n includes the noise due to the thermal emission from the surrounding environment, the receiver noise and the noise due to the lossy antenna. The reader can refer to (Hayne, 1980; Rodriguez, 1988) for a mathematical formulation of the pulse limited altimeter in the presence of a rough sea surface superimposed to a spherical Earth and in the presence of antenna mispointing errors.

3.2. The external calibration approach

Transponder calibration is based on the comparison between the theoretical power at the output of the altimeter instrument when it captures the impulse emitted by the transponder, and the actual power detected by the instrument as produced by the RA-2 level 1b (L1B) processing software. A discrepancy between the two indicates a wrong value of the overall instrument gain considered within the processing chain. The nominal value of the latter is determined on the bases of the on ground characterisation of the instrument and the on board internal PTR calibration (i.e., estimated ε^F). The level 1 processing chain used in the framework of this activity is the Envisat Instrument Engineering Calibration Facility (IECF) processor run at the ESA ESRIN processing facility (Roca and Francis, 1999; Celani, 2001).

The received power at the antenna output can be expressed by the standard radar equation:

$$P_r = \frac{P_t G_{RA}^2 \lambda^2 RCS}{(4\pi)^3 R^4 L} \tag{1}$$

where λ is the wavelength, P_t is the transmitted power, G_{RA} is the RA-2 antenna gain (which accounts for antenna losses A_3), R is the radar-target distance, L account for the path losses through the propagation media (the atmosphere), P_n for the additive noise power, and RCS is the Radar Cross Section of the TPD. The latter can be written as function of the TPD electronics:

$$RCS = \frac{\lambda^2 G_{TRA}^2 G_{elec}}{4\pi} \tag{2}$$

with G_{TRA} being the TPD antenna gain and G_{elec} being the overall gain of the TPD electronic devices. Assuming the RA-2 receiver scheme reported in Fig. 2 and using the terminology and symbols of the L1B processing technical documentation as reported in (Alberti, 2005), the theoretical power from the TPD at the Signal Processing Sub Assembly (SPSA) output is:

$$\begin{aligned} P_{theo} &= P_r G_{Rx} = P_t \frac{G_{RA}^2 \lambda^2 RCS}{(4\pi)^3 R^4 L} G_{Rx} \\ &= \frac{P_p}{A_T} \frac{G_{RA}^2 \lambda^2}{(4\pi)^3 R^4 L} \frac{\lambda^2 G_{TRA}^2 G_{elec}}{4\pi} \frac{\varepsilon^F G_{MR} G_{SPSA}}{A_R AGC_{sig}} \end{aligned} \tag{3}$$

where $G_{Rx} = \varepsilon^F G_{MR} G_{SPSA} / A_R AGC_{sig}$ is the overall gain of the receiver, A_R is the attenuation of the receiving path. P_r is expressed in term of the power P_p at the High Power Amplifier (HPA) and the attenuation A_T of the transmitting path ($P_r = P_p/A_T$). The attenuation terms in Eq. (3) can be written as function of the path losses of the antenna waveguides and the Front End Electronics (FEE; see Fig. 2):

$$A_R = A_1 A_2 A_4'; \qquad A_T = A_1 A_2 A_4'' \tag{4}$$

By introducing the product of the various path attenuations $\varepsilon^G = A_R A_T$, the Eq. (3) can be rewritten in a more synthetic form as in the following:

$$\begin{aligned} P_{theo} &= \frac{P_P G_{RA}^2 \lambda^4 \varepsilon^F G_{MR} G_{SPSA} G_{TRA}^2 G_{elec}}{AGC_{sig} (4\pi)^4 R^4 L \varepsilon^G} \\ &= \frac{G_{TX-RX}}{AGC_{Ku}} \frac{G_{RA}^2 \lambda^4 G_{TRA}^2 G_{elec}}{(4\pi)^4 R^4 L} \end{aligned} \tag{5}$$

where the AGC setting for the Ku band, named AGC_{Ku}, combines the actual value of the AGC attenuator (AGC_{sig}), the various path attenuations and the PTR calibration factor ε^F, and the terms G_{MR}, G_{SPSA} and P_P are combined in a single gain factor $G_{TX\text{-}RX}$ according to the following:

$$AGC_{Ku} = \frac{AGC_{sig}}{\varepsilon^F} \varepsilon^G; \qquad G_{TX-RX} = P_P G_{MR} G_{SPSA} \tag{6}$$

Despite the use of the formalism related to the Envisat RA-2 L1B data processing, the above formulation is quite general and can be applied to any altimeter instrument.

Note that during the acquisition of several echoed waveforms the detected power changes with *time* because of the change of some of the quantities in Eq. (3) along the satellite trajectory. Namely, the time variation of the theoretical power is due to the following factors:

- The range variation during the RA-2 flying over.
- The TPD and RA-2 antenna gain variations caused by the different line of sight between the two devices during the RA-2 flying over.

The Eq. (3) can be rewritten to include such independent variables. According to the IECF documentation (Roca and Francis, 1999; Celani, 2001) the theoretical power computed within IECF and used in our calibration exercise does not include the attenuation corrected for in flight calibration and it is therefore given by the following:

$$P_{theo}^{IECF}(time) = P_{theo}(time)AGC_{Ku} = \frac{G_{TX-RX}\lambda^4 G_{RA}^2(\theta_{RA},\varphi_{RA};time)G_{TRA}^2(\theta_{TPD},\varphi_{TPD};time)G_{elec}}{(4\pi)^4 R(time)^4 L} \quad (7)$$

where θ and φ are the elevation and azimuth angles of the line of sight with respect to the altimeter (θ_{RA} and φ_{RA}) and transponder (θ_{TPD} and φ_{TPD}) antenna reference frames. A series of waveforms collected during the RA-2 overpass of the TPD have been aligned and displayed in Fig. 3, where the TPD pulses in each waveform shows, as expected, a change in amplitude, together with a change in the position within the waveform due to the change of the range.

For calibration purposes, the theoretical power has to be compared to the power P_{meas} effectively collected by the instrument when receiving the transponder echo. The echoed TPD power is derived by integrating the waveform samples $P(k)$ (i.e., summing up the outputs of the FFT forming each waveform) contained in each RA-2 Data Set record, i.e., available each 55.7 ms, from which the noise power contribution must be subtracted. Using again the formalism of the RA-2 processor documentation, without loss of generality, the following computation is performed within the IECF starting from the RA-2 L1B product:

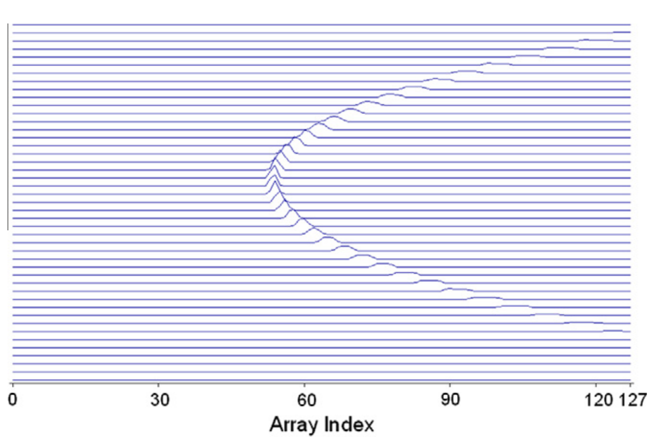

Fig. 3. Altimeter output waveforms when receiving the TPD signal in PLO mode. Several consecutive waveforms are plotted side by side and the change of amplitude and delay of the TPD received pulse can be noticed.

$$P_{meas}^{IECF}(time) = AGC_{ku}P_{meas} = \frac{AGC_{Ku}}{2048}\sum_{k=1}^{128}[P(k,time) - P_n] \quad (8)$$

where *time* refers to the acquisition of the Data Set record, $P(k)$ is the kth sample ($k = 1,....28$) of the waveform, and P_n is the instrument noise estimated from the waveforms by averaging the first K samples when the echoed signal is not present

$$P_n = \frac{1}{2048K(t2-t1)}\sum_{k=1}^{K}\sum_{time=t1}^{t2} P(k,time) \quad (9)$$

Where $t2 - t1$ indicates the range of *time* of considered Data Set records encompassing the TPD signal acquisition. The factor 2048 is a conversion factor to be applied after the Intermediate Frequency (IF) mask correction, which is not relevant from conceptual point of view. Note that the presence of AGC_{Ku} in Eq. (8) compensates its absence in Eq. (7), since the quantity simplifies when equating (7) and (8), as it will be observed later on.

The final step of the calibration procedure is the estimation of the *Bias*, which is defined by the following:

$$P_{meas}(time) = Bias \cdot P_{theo}(time)$$
$$P_{meas}(time)|_{dB} = Bias|_{dB} + P_{theo}(time)|_{dB} \quad (10)$$

Using (7) and (8), Eq. (10) becomes:

$$P_{meas}^{IECF}(time) = \frac{AGC_{Ku}}{2048}\sum_{i=1}^{128}[P(k,time) - P_n] = \\ = Bias \cdot \frac{G_{TX-RX}\lambda^4 G_{RA}^2(\theta_{RA},\varphi_{RA};time)G_{TRA}^2(\theta_{TPD},\varphi_{TPD};time)G_{elec}}{(4\pi)^4 R(time)^4 L} \\ = Bias \cdot P_{theo}^{IECF}(time) \quad (11)$$

The *Bias* includes all the constant unknowns (or poorly known) which appear in Eq. (11). The estimation of the *Bias* is performed by means of a linear regression between the RA-2 measured power and the theoretical one using all the Data Set records (i.e., all values of *time* between $t1$ and $t2$ introduced before) where the TPD pulse was detectable. The scatter plot between the measured and theoretical power is fitted by the bisector line, that is the fitting line is constrained to cross the origin of the plot.

The computation of $R(time)$, $G_{RA}(time)$ and $G_{TRA}(time)$ is of course a critical step of the overall procedure. It requires an accurate knowledge of the antenna position and pointing, as well as the shape of the antenna pattern (both of the TPD and RA-2), in order to compute R and the line-of-sight zenith and azimuth angles with respect to the satellite and to the transponder reference frames. We do not go into details on these procedures, which are quite standard in the domain of satellite data processing. We just point out that the elevation and azimuth angles are derived by the Doppler Orbitography and Radio-positioning Integrated by Satellite (DORIS) intermediate orbit (Auriol and Tourain, 2010; Jayles et al., 2010), that is by knowing at a certain time the position of the satellite and, obviously, the fixed position of the transponder on ground. The value of the gain is then extracted from the antenna patterns, which have been characterized on ground by standard techniques. In order to compute $R(time)$, we estimate the arrival time of the transponder signal in the altimeter waveform using the RA-2 ranging capability itself. It can be done by computing the pulse barycentre position in the waveform after having subtracted the noise level. Subsequently, the range as function of time can be reconstructed from the *window time delay* extracted from L1B product and *Doppler shift*, compensated for the *time delay predicted rate* which accounts for the platform vertical velocity and produces a *flattened* range estimate. The latter compensation accounts for the time difference between the RA-2 closest approach to the TPD and the closest point to the TPD nadir. However, the main factors determining the temporal trends in Fig. 4 are the two antenna gains, and an error in the range of the order of meters does not influence too much the final bias estimation. We have verified that even the consideration of the DORIS Precise Orbit State Vector product does not have a significant impact.

We report here a couple of examples to better illustrate the procedure. The analyzed data concern two acquisitions, one ascending orbit (orbit number 23916, 26th September 2006) and one descending orbit (orbit number 16795, 17th May 2005). Left panels of Fig. 4 show the superimposition of the various time dependent quantities, namely the theoretical and measured powers and the range (the latter being scaled and reversed for graphical representation reasons).

A critical point, which deserves more attention in the future for improving the performances of backscatter calibration of upcoming satellite altimeters, concerns a misalignment observed between the theoretical and the measured powers. This misalignment can be noticed in the left panels of Fig. 4, and can be better appreciated in the right panels of the same figure, where the scatter plots between the two powers are displayed. This phenomenon is present for both ascending and descending acquisitions and it is noticeable that in both cases the time evolution of the theoretical power seems to be anticipated with respect to the measured one, and both are not centered with respect to the curve of the range. It is noticed that the shift is in the order of 3–4 time steps, each one corresponding to the 55.7 ms of the RA-2 Data Set record. Considering that "a 5–10 μs systematic offset exists for DORIS time" (see Zelensky et al., 2006), the time tagging error cannot justify the observed shift. If we exclude a large systematic error between DORIS orbit and RA-2 timing, a wrong consideration of the delay between closest approach and nadir

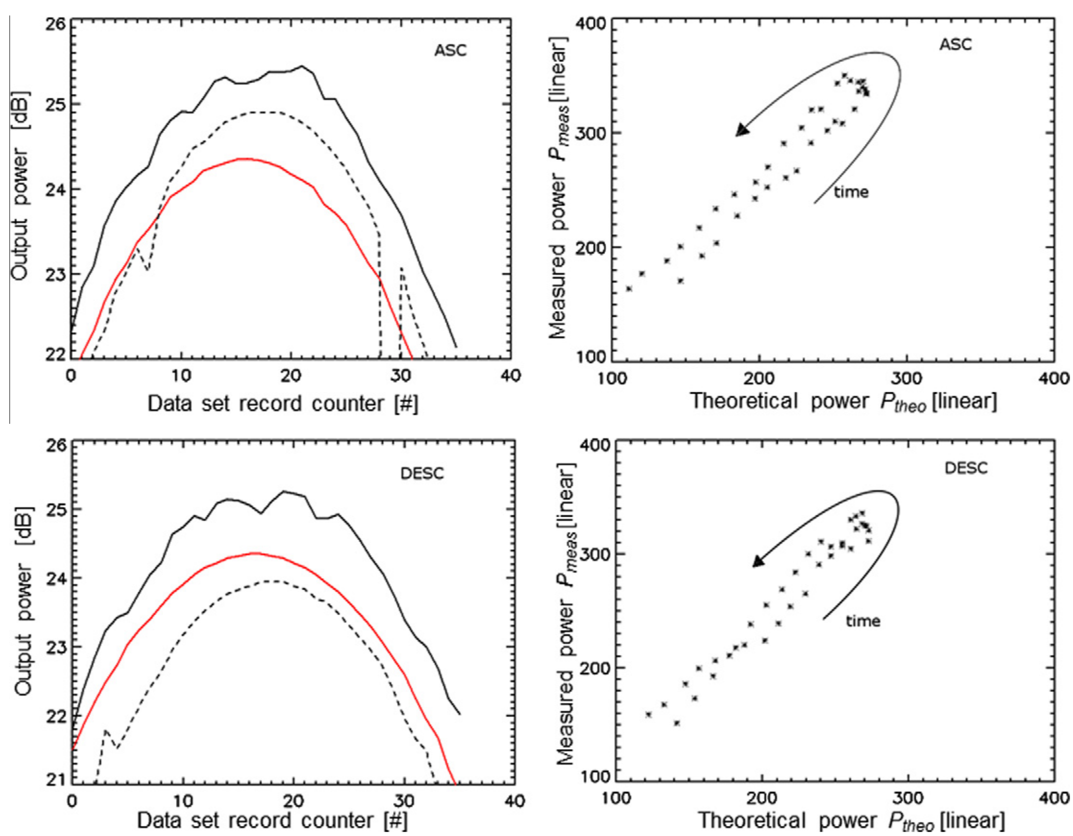

Fig. 4. Right panels: theoretical power P_{theo} (x axis) and measured power P_{meas} (y axis) scatter plots in linear units. Left panels: RA-2 powers (in dB) and range R plotted as function of time. White continuous line represents power measured values P_{meas}, yellow continuous lines represents theoretical values P_{theo} and dashed line are the range R values scaled for graphic representation purposes. Top and bottom panels refer to the ascending and descending orbit, respectively.

point must also be excluded, since it would produce opposite shifts for ascending and descending orbits being the *time delay rate* of opposite sign. In conclusions, the misalignment of the theoretical power as function of time with respect to the measured one is probably caused by a systematic error in the pointing of the antenna, either of RA-2 or the TPD, with respect to the nominal one, or a wrong characterization of the antenna patterns. Clearly, the misalignment may affect the estimation of the bias. The fitting procedure partially compensate for that misalignment, since it accounts for both branches of the plot, corresponding to the RA-2 approaching or going away from the TPD. An evaluation of the effect of such misalignment has been done by fitting a parabola with its replica shifted 4 time steps apart (similar to the shift of the TPD measurements with respect to the theoretical values). We obtained a very small difference with respect to the bias estimated without any shift, equal to about 0.05 dB. Nonetheless, this is something to be considered in the future to improve the calibration quality.

According to Eq. (10) and (11), and assuming that the additive noise power has been correctly subtracted from the altimeter output, the best fitting line should pass through the origin. To clarify the concept, Fig. 5 shows the scatterplot of the measured power as function of the theoretical one, with its symmetric replica, with superimposed the best fit line. Actually, the data points are not always aligned along a line approaching the origin, as it is apparent for instance in the upper right panel of Fig. 4, which refers to an ascending orbit. Without imposing the origin crossing, the slope of the fitting line would provide a slightly different *Bias*, with difference up to a few fractions of dB. There is not a reliable explanation for this yet, since it could be related of course to a wrong estimation of the noise, as well as to other effects, including nonlinearities. One could estimate the noise from the fitting line intercept, but this was not considered reliable, so that

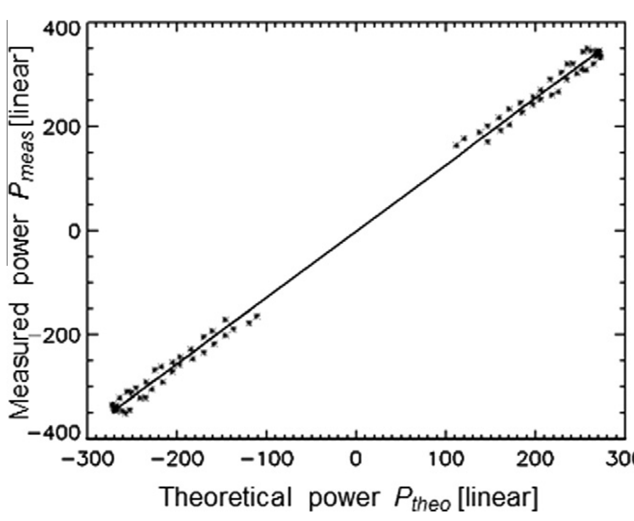

Fig. 5. Theoretical power P_{theo} (x axis) and Measured power P_{meas} (y axis) fitted by a straight line crossing the origin for bias evaluation.

the phenomena will contribute to the overall calibration uncertainty, and is another issue to be further investigated for future altimeter calibration.

3.3. The tropospheric corrections

As mentioned before, it is necessary to account for the attenuation L due to the atmosphere at Ku band. In the absence of a dedicated ground based microwave radiometer (the radiometer on board Envisat provides reliable estimates only over ocean), the theory of radiative transfer for a non-scattering horizontally stratified atmosphere in local thermodynamic equilibrium has been applied to compute the attenuation at Ku band. Profiles of atmospheric thermodynamic variables as function of height z (temperature T, pressure p and relative humidity R_h) are required to run the radiative transfer model and compute the atmospheric opacity τ (in Np), which at zenith is defined as follows:

$$\tau(f) = \int_0^\infty \alpha(f, z) dz \quad (12)$$

where f is the frequency, $\alpha(f, z)$ is the atmospheric volume absorption coefficient (Np km^{-1}) and z is the height of the emitting air volume (km); when considering observations along slanted paths, the simple secant mapping function can be used. We have used as input data the vertical profiles of atmospheric variables (T, p, R_h) provided by the European Centre for Medium-Range Weather Forecasts (ECMWF), both atmospheric analysis and forecasts at synoptic hours. In our computations the *Liebe* (Liebe, 1985) water vapor and oxygen absorption model and the Decker et al. (1978) cloud model, exploiting a relationship between cloud thickness and cloud water density, have been used to compute $\alpha(f, z)$ from the atmospheric profiles. These algorithms are valid for frequencies below 100 GHz in the absence of precipitating hydrometeors.

The ECMWF profiles have been collected at 16 pressure levels at 6 am (analysis), 9 am (forecast) and 12 am (analysis) for the daily Envisat passes, in a grid point as much close as possible to the transponder location. To better approximate a continuous atmosphere, profiles have been extrapolated to 0.1 hPa and interpolated between available levels (Schroeder and Westwater, 1991). As for the evening passes, the corresponding times are 6 pm, 9 pm., and 12 pm. The three values of atmospheric transmittances have been combined depending on the observation of the meteorological conditions at the Envisat overpass reported by the operators on the campaign form. Generally, for stable conditions the three attenuation values have been averaged, while for unstable conditions the closest in time has been used. When cloudy conditions were indicated by the operators in the campaign form, the ECMWF profiles classified as clear-sky have been disregarded, whilst the opposite criterion has been adopted in case the operators registered clear conditions. The 1-way attenuations computed in this way were reported in Table 1.

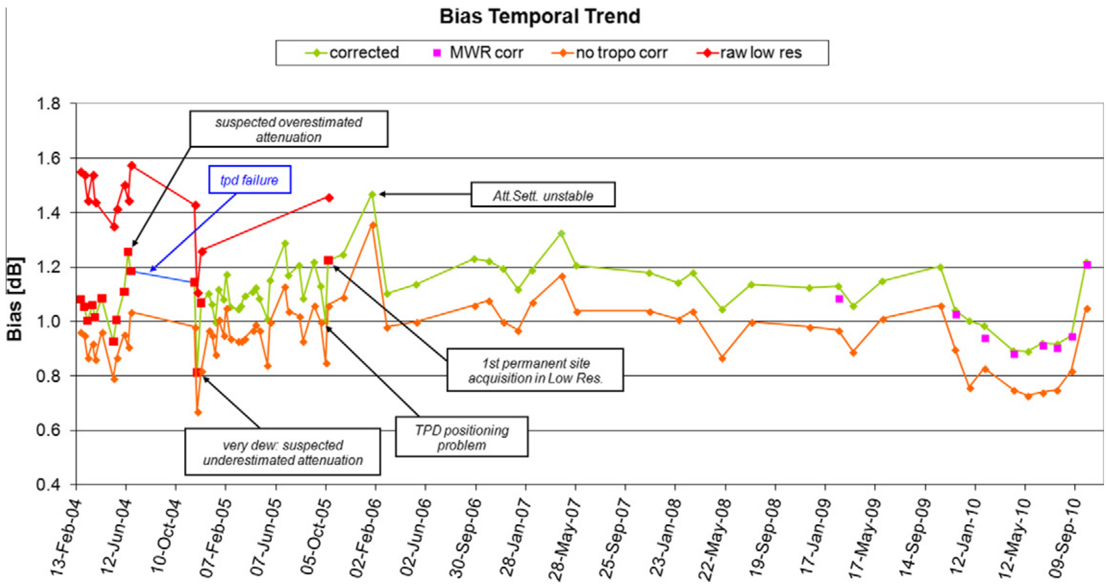

Fig. 6. Overall history of the *Bias* estimates as function of the time, both with (green diamond and line) and without (orange diamond and line) tropospheric corrections and without application of the PTR for data collected in Low Resolution (red diamond). The pink square symbols refer to correction of the tropospheric attenuation based on a ground based radiometer located about 3 km far from the TPD and operated only during the last calibration campaigns. Data points where the estimated value is considered not reliable are pointed out. (For interpretation of color in Fig. 6, the reader is referred to the web version of this article.)

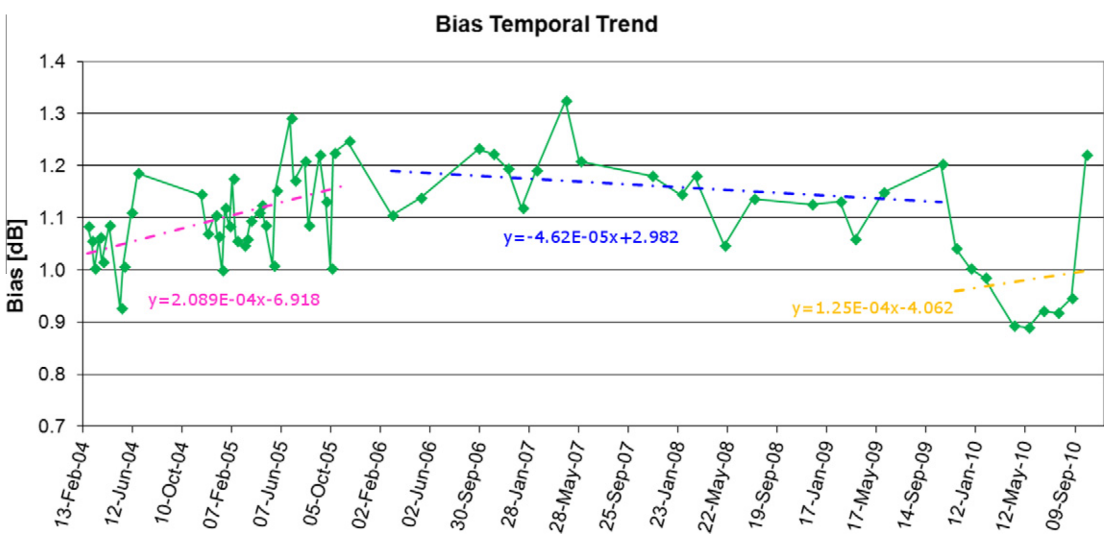

Fig. 7. Overall history of the most reliable *Bias* estimates, with superimposed the regression lines for the time periods exhibiting apparently different trends.

4. The calibration results

4.1. Bias estimation history

The bias (in decibels) is defined as the measured minus the theoretical power at the RA-2 output. Then a positive value means that the L1B processing is computing a power which is too high. If the *Bias* (i.e., the overall gain of the RA-2 instrument) increases for any reason during the mission lifetime, the RA-2 product would overestimate the sigma naught and underestimate the wind speed even if an empirical algorithm is used. All the successfully bias estimations from the beginning of the TPD acquisitions activity until the end of the mission are shown in Fig. 6. The figure reports the bias obtained before and after the application of the two-way tropospheric attenuation. A specific discussion is worth for the points collected in low resolution (LO) mode. In fact, the PTR calibration is not applied in LO mode, so that the bias would be overestimated without taking any corrective action (the PTR ε^F has usually a positive value), as shown by the red diamond in Fig. 6, which are reported for sake of completeness. For this purpose the value of PTR available in tracking mode at the closest time has been read from the data and subsequently applied, leading to the correct bias estimation represented as red squares in the same figure. Some peculiar conditions which have been encountered during operations are also indicated in the figure, thanks also to the campaign forms and pictures taken by the operators during each campaign. They helped us in selecting the more reliable points, since for instance the presence of dew on the TPD antenna or unstable values of the TPD attenuation setting are often associated to bias estimates out of its typical range.

The overall mean value of the Bias, without taking into account the points identified as suspected, equals 1.101 dB, and a regression line has been evaluated from the overall history, resulting in the following expression:

$$Bias = -2.096 * 10^{-5} * time + 1.918 \quad (13)$$

where time is expressed in days, counted starting from 1st January 1900. The overall regression line shows a very stable behavior of the RA-2 calibration, with a small negative trend, which corresponds to a variation around the mean of about 0.05 dB along the entire period of time (2415 days). The standard deviation of the bias is 0.096 dB, which is satisfactory when compared to the requirement of 0.2 dB for the calibration accuracy mentioned in Section 1. A more accurate analysis of the bias history allows one to point out some apparent variations of the bias temporal behavior. In particular, in the first period we can observe an apparent continuous increase of the bias, which probably lasted until the beginning of 2006. Then there is a very stable period, until the bias estimates obtained in the period between December 2009 and August 2010, which shows a sharp and apparently anomalous decrease up to about 0.25 dB. This jump is the main responsible for the overall negative trend shown by the best fitting line of Eq. (13). The last acquisition over the TPD (5th of October 2010) shows again a value in the order of 1.2 dB that was similar to what found for most of the time, before the anomalous jump. Unfortunately, the orbit change of Envisat that took place on 22nd of October 2010 did not allow us to further analyze this behavior. Fig. 7 shows these different phases of the overall history, pointing out only the reliable bias estimates and the fitting lines for each identified period of time, which are resumed in Table 2.

We have already discussed some sources of errors in our calibration procedure, besides the requirements of the TPD design (Jackson, 2002), which stated for the Radar Cross Section (RCS) stability a value of 0.1 dB and as for the RCS absolute calibration accuracy a value of 0.2 dB. In order to estimate an overall uncertainty of our bias estimates (at least its random component), we have analyzed statistically the differences between the individual bias estimates and the best fitting lines as function of time, which represent the final outcome of our work to be delivered to the final users. The standard deviation of the differences are reported in the last column of Table 2. If we refer to the single fitting line the error standard deviation is 0.095 dB, whereas if we trust with the piecewise approximation (i.e., the three different fitting lines) the error standard deviation is 0.071 dB. These results are of the same order of magnitude of the expected stability of the TPD. This is not surprising, as the TPD design was quite accurate, so that in conclusion the combination of errors introduced by the processing and the random TPD fluctuations still matches the initial requirement in term of stability. Conversely, as far as the absolute accuracy is concerned, we have not an independent reference to compare with, so that we have to trust on the TPD design which was based on a 0.2 dB accuracy.

Table 2
Mean value, best fitting line slope and intercept of the bias for different time frames identified in Fig. 7. Slope and Intercept refer to a linear temporal trend like in Eq. (13), where *time* is expressed in days, counted starting from 1st January 1900.

Time frame	Slope (dB/day)	Intercept (dB)	Mean bias (dB)	Error standard deviation (dB)
24/02/2004 to 05/10/2010	−2.096E−05	1.918	1.010	0.095
24/02/2004 to 15/10/2005	+2.089E−04	−6.918	1.099	
28/02/2006 to 20/10/2009	−4.619E−05	2.982	1.162	0.071
24/11/2009 to 05/10/2010	1.2509E−04	−4062	0.979	

4.2. Discussion of the results

The apparent trend pointed out in Fig. 7 should describe the drift of the radar altimeter overall gain, which is not accounted for by the internal PTR calibration. This result can be a contribution to future exploitation of RA-2 data, in view of novel and more advanced applications of the backscatter measurements, reconsidering the full historical set of geophysical products. It is understood that we could also hypothesize the possibility of a drift of the transponder itself, or problems in the method used to process the RA-2 acquisitions over the TPD and extract the bias. For instance, we have verified that the TPD attenuation factor has certainly an effect on the TPD emitted power, leading to anomalous values of the estimated *Bias*, that we have generally successfully identified on the bases of the operator report and filtered out from the full bias history. It must be said that it is not easy to resolve for this uncertainty, since there are not additional references to assess our results. One possibility is to investigate if the activity performed in the framework of RA-2 geophysical validation by different Institutions may give some useful indications, considering that wind speed is the main parameter derived from sigma naught. In particular, one could refer to the work performed in the frame of the ESA Altimetry Quality Working Group (QWG). This is of course something which is beyond the scope of our work and the interested reader should refer to the publications of the participants to the QWG for further details and investigations. Nevertheless, we would like to add some considerations based on the work of the QWG we are aware, which was gathered in the form of private communications or workshop presentations. For instance, a long term analysis of the sigma naught product performed by ECMWF (Dr. Janssen private communication) shows that none long term drift can be observed, in line with our results; this however is based on an average over the entire globe, and, above all, does not represent a proof of the stability of the altimeter, since the temporal stability of the global wind cannot be assumed *a priori*. It is interesting to note that, again in the ECMWF analysis, a drop in the global Ku backscatter has been observed at the end of year 2009, which seems to be correlated to the drop in the bias observed in Fig. 7 approximately at the same time (Abdalla, 2011). This observation does not provide a final proof, but just an indication for future investigations.

For our purpose it would be more relevant to analyze the long-term behavior of the bias between wind speed provided by RA-2 and those independently measured by buoy or derived by meteorological analysis. As a general comment, it must be observed that a drift of say 0.2 dB in sigma naught roughly corresponds to 0.6 m/s of wind speed in the range from 2 to 18 m/s, so that it is not easy to appreciate it from geophysical validation efforts that generally are based on mean global values both in time and space. This is however a topic planned for future investigations.

5. Conclusions

The paper has reviewed the entire effort carried out to perform the external calibration of the Envisat altimeter backscatter product by means of a dedicated transponder device. The methodology adopted to estimate the bias (in dB) to be applied to the currently released products has also been described. From the results of this activity we can conclude that the RA-2 was quite stable in terms of sigma naught measurements, even if a bias of about 1 dB should be considered with respect to the actually released product. Some small changes in the bias as function of time can be identified during most of the Envisat lifetime, consisting in a slight increase in the first two years, followed by a more stable period and a final drop observed during year 2010, until the end of the calibration activity (change in Envisat orbit). A fluctuation of the bias estimates with standard deviation in the order of 0.1 dB has probably to be considered a “noise” of the overall calibration approach, which is in line with the initial stability requirements. This noise can be due to different factors, including wrong estimation of the atmospheric attenuation, TPD problems, poor characterization of the antenna patterns used in the calibration procedure.

Considering the small magnitude of the RA-2 drift and the expected impact on the wind Level 2 product, it is not possible, at least at this stage, to confirm it on the bases of the available results coming from the geophysical validation exercises carried out by different Institutions. Nonetheless, the results of this work may provide additional information, to be taken into consideration by researchers interested in exploiting accurate altimeter backscatter products in several applications.

The experience gained with Envisat suggests recommendations for getting better backscatter products from the future altimetry missions, and particularly Sentinel 3. Namely, it is recommended to pay attention to the characterization of the antenna patterns (both of the altimeter and the transponder) required in the calibration algorithm, and to foresee the exploitation of a ground based microwave radiometer to estimate the tropospheric attenuation.

Acknowledgements

This work has been developed in the framework of ESA/ESRIN projects (Contracts N. 17752/03/I-OL and N. 22198/09/I-OL). We would like to thank the Italian Fire Brigade, Compartment of Rome, and in particular the Scuba Diver Team, who has offered its premise as permanent site of the transponder, and supported our team in the installation of the equipment. We would like to thank the participants of the ESA Altimetry Quality Working Group (QWG) for the interesting exchanges, and Dr. H. Jackson, from Serco FM BV, for his support on TPD hardware.

References

Abdalla, S. Global validation of ENVISAT wind, wave and water vapour products from RA-2, MWR, ASAR and MERIS (2008–2010), Final report for ESA, contract 21519/08/I-OL, 2011.

Alberti, G. Ra-2 algorithms specification for level 1b software prototyping, Alenia Spazio S.p.A. Technical Note, 14, 2005.

Auriol, A., Tourain, C. DORIS system: the new age. Adv. Space Res. 46 (12), 1484–1496, 2010.

Bannoura, W.J., Wade, A., Srinivas, D.N. NOAA ocean surface topography mission Jason-2 project overview. Proc. MTS/IEEE Oceans, 3. Silver Spring, MD, USA, pp. 2155–2159, 2005.

Barrick, D., Swift, C. The Seasat microwave instruments in historical perspective. IEEE J. Oceanic Eng. 5 (2), 74–79, 1980.

Bramer, S.M.S., Berry, P.A.M. Soil surface moisture from EnviSat RA-2: from modelling towards implementation. Int. Assoc. Geod. Symposia 1135 (3), 205–212, 2010.

Bramer, S.M.S., Berry, P.A.M., Johnson, C.P.D. Analysis of Envisat RA-2 backscatter over natural land calibration targets, in: Proc. 2004 Envisat and ERS Symposium, Salzburg, Austria, (ESA SP-572), 2005.

Brogioni, M., Pettinato, S., Macelloni, G., Paloscia, S., Pampaloni, P., Pierdicca, N., Ticconi, F. Sensitivity of bistatic scattering to soil moisture and surface roughness of bare soils. Int. J. Remote Sens. 31 (15), 4227–4255, 2010.

Celani, C. Envisat-1 instrument calibration detailed processing module, Telespazio S.p.A Technical Note, 2 (3), 2001.

Decker, M.T., Westwater, E.R., Guiraud, F.O. Experimental evaluation of ground-based microwave radiometric sensing of atmospheric temperature and water vapor profiles. J. Appl. Meteor. 17, 1788–1795, 1978.

Elfouhaily, T., Vandemark, D., Gourrion, J., Chapron, B. Estimation of wind stress using dual-frequency TOPEX data. J. Geophys. Res. 103 (C11), 25.101–25.108, 1998.

Envisat Project Team, The Envisat Mission, ESA SP-1255, 1, 2001.

Faugere, Y., Dorandeu, J.F., Lefevre, F., Picot, N., Fèmènias, P. Envisat ocean altimetry performance assessment and cross-calibration. Sensors 6, 100–130, 2006.

Fèmènias, P., Martini, A., Roca, M., Pierdicca, N., Bignami, C., Fascetti, M., Mazzetta, M. ENVISAT RA-2 Sigma-0 absolute calibration: phases and results, in: Proc. ENVISAT and ERS Symposium, Salzburg, Austria, 2004.

Frew, N.M., Glover, D.M., Bock, E.J., McCue, S.J. A new approach to estimation of global air-sea gas transfer velocity fields using dual-frequency altimeter backscatter. J. Geophys. Res. 112, C11003–C11023, 2007.

Gommenginger, P., Srokosz, M.A., Challenor, P.G., Cotton, P.D. Measuring ocean wave period with satellite altimeters: a simple empirical model. Geophys. Res. Lett. 30 (22), 2150–2154, 2003.

Gourrion, J., Vandemark, D., Bailey, S., Chapron, B., Gommenginger, G.P., Challenor, P.G., Srokosz, M.A. A two-parameter wind speed algorithm for Ku-band altimeters. J. Atm. Oceanic Tech. 19 (12), 2030–2048, 2002.

Hayne, G.S. Radar altimeter mean return waveforms from near-normal-incidence ocean surface scattering. IEEE Trans. Ant. Prop. 28 (5), 687–692, 1980.

Jackson, H. ENVISAT RA-2 transponder test & calibration report, ESA Technical note, 1, 2002.

Jayles, C., Chauveau, J.P., Rozo, F. DORIS/Jason-2: better than 10 CM on-board orbits available for near-real-time altimetry. Adv. Space Res. 46 (12), 1497–1512, 2010.

Karaev, V.Y., Kanevsky, M.B., Meshkov, E.M., Cotton, D., Gommenginger, C. Retrieval of the surface wind speed from satellite radio-altimeter data. Radiophys. Quantum Electron. 49 (4), 251–263, 2006.

Liebe, H.J. An updated model for millimeter propagation in moist air. Radio Sci. 20, 1069–1089, 1985.

Martini, A., Pierdicca, N., Bignami, C., Greco, B., Roca, M., Jackson, H., Fèmènias, P., Celani, C., Loddo, C.N. ENVISAT Ra-2 Sigma-0 absolute calibration, methods and results, in: 15 Years of Progress in Radar Altimetry Symposium, Venice, Italy, 2006.

Papa, F., Legresy, B., Mognard, N.M., Josberger, E.G., Remy, F. Estimating terrestrial snow depth with the Topex–Poseidon altimeter and radiometer. IEEE Trans. Geosci. Remote Sens. 40 (10), 2162–2169, 2002.

Papa, F., Legresy, B., Remy, F. Use of the Topex–Poseidon dual-frequency radar altimeter over land surfaces. Remote Sens. Environ. 87, 136–147, 2003.

Papa, F., Prigent, C., Rossow, W.B., Legresy, B., Remy, F. Inundated wetland dynamics over boreal regions from remote sensing: the use of Topex–Poseidon dual-frequency radar altimeter observations. Int. J. Remote Sens. 27 (21), 4847–4866, 2006.

Pierdicca, N., Greco, B., Bignami, C., Ferrazzoli, P., Mattioli, V., Pulvirenti, L. The calibration of the Envisat radar altimeter receiver by a passive radiometric technique. IEEE Trans. Geosci. Remote Sens. 44 (11), 3297–3307, 2006.

Quartly, G.D. Monitoring and cross-calibration of altimeter σ through dual-frequency backscatter measurements. J. Atm. Oceanic Tech. 17, 11252–11258, 2000.

Queffeulou, P. Long term quality status of wave height and wind speed measurements from satellite altimeters, in: Proc. 13th Int. Offshore and Polar Eng. Conf. (ISOPE), Honolulu, Hawaii, USA, 2003.

Resti, A., Benveniste, J., Roca, M., Levrini, G., Johannessen J. The ENVISAT Radar Altimeter System (RA-2), ESA Bulletin, 98, 1999.

Ridley, J., Strawbridge, F., Card, R., Phillips, H. Radar backscatter characteristics of desert surface. Remote Sens. Environ. 57 (2), 63–78, 1996.

Roca, M., Francis, R. RA-2 In-Orbit absolute calibration plan: Sigma-0, PO-PL-ESA-GS-0900,1999.

Roca, M., Jackson, H., Celani, C. RA-2 Sigma-0 absolute calibration, in: Proc. of Envisat Validation Workshop, Frascati, Italy, (ESA SP-531, August 2003), 2002.

Rodriguez, E. Altimetry for non-Gaussian oceans: height biases and estimation of parameters. J. Geophys. Res. 93 (C11), 114107–114120, 1988.

Schroeder, J.A., Westwater, E.R. Users' Guide to WPL Microwave Radiative Transfer Software, NOAA Technical Memorandum ERL WPL-213, 1991.

Seitz, B., Mavrocordatos, C., Rebhan, H., Nieke, J., Klein, U., Borde, F., Berruti, B. The sentinel-3 mission overview, in: Proc. IEEE Int. Geosci. Remote Sens. Symp. IGARSS 2010, Honolulu, Hawaii, USA, pp. 4208–4211, 2010.

Tran, N., Zanife, O.Z., Chapron, B., Vandemark, D., Vincent, P. Absolute calibration of Jason-1 and Envisat altimeter Ku-band radar cross sections from cross comparison with TRMM precipitation radar measurements. J. Atm. Oceanic Tech. 22 (9), 11389–11402, 2005.

Tran, N., Chapron, B., Vandemark, D. Effect of long waves on Ku-band ocean radar backscatter at low incidence angles using TRMM and altimeter data. IEEE Geosci. Remote Sens. Lett. 4 (4), 542–546, 2007.

Vandemark, D., Chapron, B., Sun, J., Crescenti, G.H., Graber, H.C. Ocean wave slope observations using radar backscatter and laser altimeters. J. Phys. Oceanogr. 34, 2825–2842, 2004.

Yang, L., Du, H., Ma, H., Liu, Q. Use of the merged dual-frequency radar altimeter backscatter data over china land surface, in: Proc. IEEE Int. Geosci. Remote Sens. Symp. IGARSS 2010, Honolulu, Hawaii, USA, 2010.

Yurchak, S. Assessment of specular radar backscatter from a planar surface using a physical optics approach. Int. J. Remote Sens. 33 (20), 6446–6458, 2012.

Zelensky, N.P., Berthias, J.P., Lemoine, F.G. DORIS time bias estimated using Jason-1, TOPEX/Poseidon and ENVISAT orbits. J. Geod. 80 (8–11), 497–506, 2006.